

# Probing patchy reionization through $\tau$ -21cm correlation statistics

P. Daniel Meerburg<sup>1,\*</sup>, Cora Dvorkin<sup>2,†</sup> and David N. Spergel<sup>1,‡</sup>

<sup>1</sup>*Department of Astrophysical Sciences, Princeton University, Princeton, NJ 08540 USA. and*

<sup>2</sup>*Institute for Advanced Study, Einstein Drive, Princeton, NJ 08540, USA*

(Dated: December 2, 2024)

We consider the cross-correlation between free electrons and neutral hydrogen during the epoch of reionization. The free electrons are traced by the optical depth to reionization  $\tau$  while the neutral hydrogen can be observed through 21 cm photon emission. As expected, this correlation is sensitive to the detailed physics of reionization. Foremost, if reionization occurs through the merger of relatively large halos hosting an ionizing source, the free electrons and neutral hydrogen are anti-correlated for most of the reionization history. A positive contribution to the correlation can occur when the halos that can form an ionizing source are small. A measurement of this sign change in the cross-correlation would directly measure the bubble bias and as, such, the halo mass. We estimate the signal-to-noise of the cross-correlation using the estimator for inhomogeneous reionization  $\hat{\tau}_{\ell m}$  proposed by Dvorkin and Smith (2009). We find that with upcoming radio interferometers and CMB experiments, the cross-correlation is measurable going up to multipoles  $\ell \sim 1000$ . We also derive parameter constraints and conclude that, despite the foregrounds, the cross-correlation proofs a complementary measurement of the EoR parameters to the 21 cm and CMB polarization auto-correlations expected to be observed in the coming decade.

## I. INTRODUCTION

The epoch of reionization (EoR) is one of the least understood periods of cosmic history, with only limited observational measurements (see e.g. [1]). The absence of the Gunn-Peterson trough in the spectra of quasars implies that reionization should have been completed around  $z = 6$  [2, 3]. The total optical depth to reionization has been measured to be  $\tau = 0.084 \pm 0.013$  [4]. If reionization is assumed to be instantaneous, this would imply a transition redshift of  $z_{\text{re}} = 11$ . Besides these constraints, we know very little about the details of reionization, such as the typical halo mass associated with the first ionizing objects as well as the distribution of these objects inside the halos.

The spectral mapping of neutral hydrogen in emission [5–11] promises to be a new probe of the EoR. The spontaneous hyperfine spin flip transition causes the emission of a photon with a wavelength of 21 centimeters in the rest frame. Applying different base filters to the observed emission, it is possible to map the distribution of neutral hydrogen in the Universe as a function of redshift. The auto-correlation of the observed maps is very sensitive to the EoR parameters.

Additionally, cross correlating the observed maps with other observables could provide complementary constraints on the EoR parameters. For example, the 21 cm fluctuations are expected to be correlated with galaxies [12, 13] as well as with the Cosmic Microwave Background (CMB) fluctuations through the Doppler peak and the kinetic SZ effect (see e.g. [14–18] and [19] for

recent simulations). Unlike the fluctuations in 21 cm, which are a direct representation of the underlying neutral hydrogen, no direct measurement of the electron density at high redshifts exists. The electron density can be measured indirectly through its integrated effect on the CMB, providing us with a number ( $\tau$ ) that tells us the fraction of photons affected by scattering of electrons along the line of sight. One can go further and reconstruct the inhomogeneities in the optical depth field by considering second order effects on the CMB due to the screening mechanism [20], Thomson scattering and the kSZ effect (see Ref. [21], where an estimator of the anisotropic optical depth field is derived and Ref. [22] for an implementation of this estimator to WMAP 7-year data). In this work we consider the cross-correlation between a reconstructed map of the inhomogeneous optical depth  $\tau_{\ell m}$  (using CMB polarization observations) and a neutral hydrogen map measured through the redshifted 21 cm lines. Intuitively, these two observables are expected to be anti-correlated on most scales.

Besides providing complementary constraints on the EoR parameters, the cross-correlation between the 21 cm field and the CMB should in principle be less sensitive to the details of the foregrounds. Although current [23, 24] and upcoming experiments [25, 26] are expected to be capable of measuring the auto-correlation of 21 cm maps, one very persistent nuisance in extracting the signal from reionization are the foregrounds. Inhomogeneities in the 21 cm signal due to patchy reionization must be separated from fluctuations in foreground sources. Typical foreground sources are faint radio galaxies, starburst galaxies and galaxies responsible for reionization. In addition, our own Galaxy is very bright at the frequencies one aims at for mapping the 21 cm signal from reionization, exceeding the 21 cm reionization signal by several orders of magnitude. Attempts have been made to characterize these foregrounds [27, 28]. Despite these efforts,

\*Electronic address: meerburg@princeton.edu

†Electronic address: cdvorkin@ias.edu

‡Electronic address: dns@astro.princeton.edu

foregrounds can never be fully removed, simply because we do not know their exact origin.

This paper is organized as follows. We review the physics of reionization and derive the expressions for the fluctuations in 21 cm  $a_{\ell m}^{21}$  and fluctuations in the optical depth  $\tau_{\ell m}$  in §II. The former is proportional to the neutral hydrogen fraction, while the latter is proportional to the free electron fraction. Using a simple reionization model [10, 29] where regions of HII are represented by spherical bubbles of typical size  $\bar{R}$  we derive an expression for the cross-correlation  $\langle \tau_{\ell m} a_{\ell m}^{21*} \rangle$  in section §III. In §IV and §V we study the 1-bubble and 2-bubble contributions to the power spectrum. We compute the angular power spectrum of the cross-correlation in §VI. We assess the observability of the cross correlation by using a redshift weighting to maximize the signal to noise. We end this section with an estimate of the EoR parameter constraints, when considering LOFAR and SKA noise levels. We present our conclusions in §VIII. In the Appendix we discuss the dependence of the cross-correlation on the parameters of the reionization model.

Unless specifically mentioned, we use the following set of parameter values throughout the paper:  $h = 0.704$ ,  $\Omega_b = 0.044$ ,  $\Omega_c = 0.23$ ,  $\Omega_K = 0$ ,  $n_s = 0.96$  and  $\tau = 0.084$ . Lensing is included and we use the non-linear halo fit model to determine the power spectrum of density fluctuations. We use the WMAP pivot scale  $k_* = 0.002 \text{ Mpc}^{-1}$  and  $A_s = 2.46 \times 10^{-9}$  [4].

## II. 21 CM BRIGHTNESS AND THE OPTICAL DEPTH TO REIONIZATION

In this section we will review the standard results for fluctuations in the 21 cm temperature brightness and relate those to fluctuations in the neutral hydrogen fraction. In the second half of this section, we will derive the fluctuations in the optical depth  $\tau$  caused by fluctuations in the free electron fraction along the line of sight, confirming the results first obtained in [18].

The optical depth of a region of the IGM in the hyperfine transition is given by [30]

$$\tau_{21}(z) = \frac{3c^3 h A_{10}}{32\pi k \nu_0^2 T_S} \frac{n_{HI}}{(1+z)(dv_{\parallel}/dr_{\parallel})}, \quad (1)$$

where  $\nu_0 = 1420.4 \text{ MHz}$  is the rest frame hyperfine 21 cm ( $\nu_0 = \lambda_{21}/c$ ) transition frequency,  $A_{10} = 2.85 \times 10^{-15} \text{ s}^{-1}$  is the spontaneous emission coefficient for this transition,  $T_S$  is the spin temperature of the IGM, weighting the relative population of the atoms in the singlet state to atoms in the triplet state [30],  $n_{HI}$  is the neutral hydrogen density, and  $v_{\parallel}$  the proper velocity along the line of sight. At high redshifts, where peculiar motions along the line of sight are small compared to the Hubble flow,  $dv_{\parallel}/dr_{\parallel} = H(z)/(1+z)$ . At  $z = 10$  dark energy and radiation are both unimportant and we can solve for  $H(z)$  in a matter dominated Universe,  $H(z) \simeq H_0 \Omega_m^{1/2} (1+z)^{3/2}$ .

We can now write the following expression for the optical depth:

$$\tau_{21}(z) \simeq 8.6 \times 10^{-3} (1 + \delta_b) x_H \left[ \frac{T_{cmb}}{T_S} \right] \left[ \frac{1 - Y_p}{1 - 0.248} \right] \times \left( \frac{\Omega_b}{0.044} \right) \left[ \left( \frac{0.27}{\Omega_m} \right) \left( \frac{1+z}{10} \right) \right]^{1/2} \quad (2)$$

Here we used  $T_{cmb} = 2.73(1+z)\text{K}$ ,  $\delta_b = (\rho_b - \bar{\rho}_b)/\bar{\rho}_b$  and

$$n_{HI} \simeq (1 - Y_p) x_H \frac{\Omega_b}{\Omega_m} \frac{\rho_m}{m_p},$$

where  $x_H$  is the neutral hydrogen fraction, i.e.  $x_H = n_{HI}/(n_{HI} + n_e)$ ,  $\rho_m$  is the matter energy density and  $m_p$  is the proton mass. The factor  $(1 - Y_p)$  addresses the fact that not all protons are in hydrogen, but a fraction is in Helium.

The intensity along the line of sight from a thermal source is given by

$$I = I_0 e^{-\tau} + \int_{\tau}^0 d\tau' e^{-\tau'} \frac{\eta_{\nu}}{\kappa_{\nu}}, \quad (3)$$

with  $\kappa_{\nu}$  the absorption coefficient and  $\eta_{\nu}$  the emissivity of photons. Using  $dI = \eta_{\nu} dl - \kappa_{\nu} I dl = 0$  in the Rayleigh-Jeans limit, we have  $I = 2kT_b \nu^2/c^2$ , while  $\eta_{\nu}/\kappa_{\nu} = 2kT_S \nu^2/c^2$  and  $I_0 = 2kT_{cmb} \nu^2/c^2$ . Hence, we can write the 21 cm brightness temperature as:

$$T_b = T_{cmb} e^{-\tau_{21}} + T_S (1 - e^{-\tau_{21}}) \quad (4)$$

The brightness temperature increment is defined at an observed frequency  $\nu$  corresponding to a redshift  $1+z = \nu_0/\nu$  as

$$\delta T_b(z) \equiv \frac{T_b - T_{cmb}}{1+z} \simeq \frac{(T_S - T_{cmb})}{1+z} \tau_{21} \quad (5)$$

Using Eq. (2), we can re-write Eq. (5) as [5, 7]

$$\delta T_b(z) \simeq 27 \text{ mK} (1 + \delta_b) x_H \left[ \frac{T_S - T_{cmb}}{T_S} \right] \left[ \frac{1 - Y_p}{1 - 0.248} \right] \times \left( \frac{\Omega_b}{0.044} \right) \left[ \left( \frac{0.27}{\Omega_m} \right) \left( \frac{1+z}{10} \right) \right]^{1/2} \quad (6)$$

There are usually two types of filters associated with the resolution of the experiment. First, there is a finite angular resolution, which will affect all modes perpendicular to the line of sight. Second, since the brightness temperature of the 21 cm emission is a 3-dimensional field, we are confined to a frequency resolution or bandwidth, which affects the modes along the line of sight (or, equivalently, a redshift resolution).

The total integrated 21 cm surface brightness is given by

$$T_b(\hat{n}, \chi) = T_0(\chi) \int d\chi' W_{\chi}(\chi') \psi(\hat{n}, \chi') \quad (7)$$

Here  $W_\chi$  is an experimental band filter that is due to the finite frequency resolution of the instrument, which is centered around  $\chi$  (comoving distance). We define the dimensionless brightness temperature  $\psi$  as

$$\psi = (1 + \delta_b)x_H \left( \frac{T_s - T_{cmb}}{T_s} \right) \quad (8)$$

In the limit of  $T_s \gg T_{cmb}$ ,  $\psi = (1 + \delta_b)x_H$ .

Now  $T_0(z)$  can be written as

$$T_0(z) \simeq 27 \text{ mK} \left[ \frac{1 - Y_p}{1 - 0.248} \right] \left( \frac{\Omega_b}{0.044} \right) \left[ \left( \frac{0.27}{\Omega_m} \right) \left( \frac{1+z}{10} \right) \right]^{1/2} \quad (9)$$

We will now consider fluctuations in the free electron density, which in turn will induce fluctuations in the optical depth. The optical depth to distance  $\chi$  along the line of sight is given by

$$\tau(\hat{n}, \chi) = \sigma_T \int_0^\chi d\chi' n_e(\hat{n}, \chi') a(\chi'), \quad (10)$$

where  $\sigma_T$  is the Thomson cross-section,  $n_e$  is the electron number density and  $a$  is the scale factor. Relating the free electron density to the free electron fraction  $x_e$ , we can write

$$n_e(\hat{n}, \chi) \simeq \frac{x_e \rho_b}{m_p} (1 - \frac{3}{4} Y_p), \quad (11)$$

assuming that Helium is singly ionized.

The average baryon density diffuses in an expanding background as  $a^{-3}$ , and the free electron density becomes

$$n_e(\hat{n}, \chi) = (1 - \frac{3}{4} Y_p) \frac{\rho_{b,0}}{m_p} a^{-3} (1 + \delta_b) x_e \quad (12)$$

The optical depth can in turn be written as

$$\begin{aligned} \tau(\hat{n}, \chi) &= \sigma_T (1 - \frac{3}{4} Y_p) \frac{\rho_{b,0}}{m_p} \int_0^\chi \frac{d\chi'}{a^2(\chi')} x_e(\hat{n}, \chi') \\ &\times (1 + \delta_b(\hat{n}, \chi')) \end{aligned} \quad (13)$$

Therefore, we can relate fluctuations in the optical depth  $\delta\tau$  to fluctuations in the 21 cm brightness temperature  $\delta T_b$  [18] as

$$\delta\tau = (1 - \frac{3}{4} Y_p) \frac{\sigma_T \rho_{b,0}}{m_p H_0 \Omega_m^{-1/2}} \int dz \left[ (1+z)^{1/2} \delta_b - \frac{\delta T_b(z)}{8.5 \text{ mK}} \right], \quad (14)$$

where we have assumed a delta window function.

It is worth noticing that the above expression for the fluctuations in the 21 cm brightness temperature is only valid for  $T_s > T_{\text{CMB}}$ . Early on, when the number of ionizing sources are rare and the temperature of the IGM close to these sources is coupled to the kinetic temperature by Ly $\alpha$  photons associated with these local sources, this assumption breaks down, and the 21 cm signal can appear in absorption. We neglect this effect in this paper.

### III. CORRELATING $X$ AND $\psi$

We will now cross-correlate the optical depth fluctuations with the temperature brightness. As we saw before, the CMB optical depth is proportional to the free electron density. If reionization is inhomogeneous, the free electron density is a function of position in the sky. Anisotropies in the optical depth produce three effects in the CMB: (i) screening of the temperature and polarization fluctuations that we observe today by an overall factor of  $e^{-\tau(\hat{n})}$ . This effect generates CMB B-mode polarization; (ii) Thomson scattering: new polarization is generated by scattering of the local temperature quadrupole that each electron sees along the line of sight. This effect also produces B-modes; and (iii) new temperature anisotropy is generated from the radial motion of ionized bubbles relative to the observer (the kinetic Sunyaev Zel'dovich effect).

The two-point correlation function between the E-modes and the B-modes generated from patchy reionization is proportional to the anisotropic part of the optical depth. This fact allowed the authors in Ref. [21] to write a minimum variance quadratic estimator  $\hat{\tau}_{\ell m}$  for the field  $\tau(\hat{n})$ . In this work, we will use the CMB polarization fluctuations to reconstruct a map of  $\tau$  and cross-correlate it with the 21 cm field.

We will use the shorthand notation  $X(\hat{n}, \chi) = x_e(1 + \delta_b)$ . We can write the cross-correlation between the field  $X$  (measured through the CMB) and the field  $\psi$  (measured through 21 cm) as

$$\begin{aligned} \xi_{X\psi} &\simeq -\xi_{xx}(1 + \xi_{\delta\delta}) - (\bar{x}_H - \bar{x}_e + \xi_{x\delta})\xi_{x\delta} \\ &+ (\bar{x}_H - \bar{x}_H^2)\xi_{\delta\delta} \end{aligned} \quad (15)$$

Here we defined  $\xi_{xx} = \langle x_H(\vec{x}_1) x_H(\vec{x}_2) \rangle - \bar{x}_H^2$ ,  $\xi_{\delta\delta} = \langle \delta_b(\vec{x}_1) \delta_b(\vec{x}_2) \rangle$  and  $\xi_{x\delta} = \langle \delta_b(\vec{x}_1) x_H(\vec{x}_2) \rangle$ . We make the simplistic assumption that the connected part of  $\langle \delta_x \delta_x \delta_b \delta_b \rangle$  vanishes. Here  $\delta_x$  corresponds to fluctuations in the neutral hydrogen fraction, which is given by  $x_H = \bar{x}_H (1 + \delta_x)$ .

Before we can compute  $\xi_{X\psi}$  we need to specify our model of reionization. We will assume that the Universe reionized through the growth of ionized bubbles associated with massive halos. The bubbles themselves contain a single source and we assume their size to be larger than the non-linear scale.

We will adopt the following average reionization fraction as a function of redshift

$$\bar{x}_e(z) = \frac{1}{2} \left[ 1 + \tanh \left( \frac{y_{\text{re}} - (1+z)^{3/2}}{\Delta y} \right) \right], \quad (16)$$

which is the one used in the code CAMB [31]. Here  $y(z) = (1+z)^{3/2}$ ,  $y_{\text{re}} = y(z_{\text{re}})$  and  $\Delta y$  are free parameters that satisfy our integrated optical depth along the line of sight  $\tau = 0.084$ .

The ionized bubble around a given source is assumed to be spherical with an average radius  $\bar{R}$ . We will assume

that the typical ionized bubble radii are log-normal distributed [32], i.e. there is a skewness towards smaller bubble sizes,

$$P(R) = \frac{1}{R} \frac{1}{\sqrt{2\pi\sigma_{\ln R}^2}} e^{-[\ln(R/\bar{R})]^2/(2\sigma_{\ln R}^2)}, \quad (17)$$

where  $\sigma_{\ln R}$  is the variance of the distribution.

The average bubble volume is then given by

$$\langle V_b \rangle = \int dR P(R) V_b(R) = \frac{4\pi\bar{R}^3}{3} e^{9\sigma_{\ln R}^2/2} \quad (18)$$

Hence, we can define a volume weighted radius,  $R_0$  such that  $\langle V_b \rangle = 4\pi R_0^3/3$ , which can be written as

$$R_0 = \bar{R} e^{3\sigma_{\ln R}^2/2} \quad (19)$$

If we assume that a given point in space is ionized with Poisson probability, we can write the ionization fraction as

$$\langle x_e(\vec{x}) \rangle_P = 1 - e^{-n_b \langle V_b \rangle}, \quad (20)$$

with  $n_b$  the number density of bubbles. The brackets around  $x_e$  are placed to remind us that we are considering a Poisson distribution of sources, and the result is averaged over the Poisson process. We further assume that the number density of bubbles traces the large-scale structure with some bias  $b$ :

$$n_b(\vec{x}) = \bar{n}_b (1 + b\delta_W(\vec{x})), \quad (21)$$

while the average bubble number density is related to the mean ionization fraction as

$$\bar{n}_b = -\frac{1}{\langle V_b \rangle} \ln(1 - \bar{x}_e) \quad (22)$$

The bias can in principle also be a function of  $R$  (see e.g. Ref. [29]), but for simplicity we will use a fixed value throughout this paper. We will investigate the consequence of changing the bubble bias where it is relevant.  $\delta_W$  is the matter over-density  $\delta$  smoothed by a top hat window of radius  $R$ ,

$$\delta_W(\vec{x}) = \int d^3x' \delta(\vec{x}') W_R(\vec{x} - \vec{x}') \quad (23)$$

In momentum space,

$$W_R(k) = \frac{3}{(kR)^3} [\sin(kR) - kR \cos(kR)], \quad (24)$$

which is the Fourier transform of  $W_R(x) = V_b^{-1}$  for  $x \leq R$  and  $W_R(x) = 0$  otherwise.

We further define

$$\langle W_R \rangle(k) = \frac{1}{\langle V_b \rangle} \int_0^\infty dR P(R) V_b(R) W_R(kR) \quad (25)$$

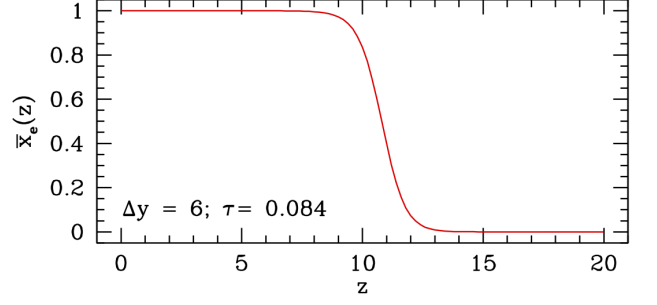


FIG. 1: The average ionization fraction  $\bar{x}_e(z)$  as a function of redshift  $z$ .

and

$$\langle W_R^2 \rangle(k) = \frac{1}{\langle V_b \rangle^2} \int_0^\infty dR P(R) [V_b(R) W_R(kR)]^2 \quad (26)$$

Throughout this paper we will consider bias  $b = 6$  and  $\Delta y = 6$ , unless otherwise specifically mentioned. For a qualitative analysis of the correlation function as a function of the parameters of our reionization model, we refer the reader to the Appendix. The average ionization fraction as a function of redshift is shown in Fig. 1, where the choice of parameters corresponds to a scenario with a neutral Universe at  $z \geq 13$  and a completely ionized Universe at  $z \leq 6$ .

#### IV. TWO BUBBLE CORRELATIONS

The cross-correlation between the neutral hydrogen and free electron fraction has two main contributions. First, the correlation is set by the Poisson distribution of ionizing sources inside the bubbles. This term is referred to as the 1-bubble term, and it is dominated by the shot noise. Second, cross correlations can also be induced by the enhanced probability of bubble formation (or ionizing sources) inside overdense regions (with probability  $\langle x_e \rangle$ ). This term is referred to as the 2-bubble term, and is relevant for scales much larger than the average size of a bubble.

In order to compute the 2-bubble correlation function, we relate the number density of bubbles to the overdensities in dark matter. We define the bubble bias, which is related to the familiar halo bias  $b_h$  via (see e.g. Ref. [29])

$$b = \frac{1}{\bar{n}_b} \int_\Lambda^\infty \frac{dM}{M} b_h(M) \frac{dn_h}{d \ln M}, \quad (27)$$

where  $dn_h/d \ln M$  represents the halo mass function.

The integral runs over all masses with some threshold mass scale  $\Lambda$ , above which halos are capable to form ionizing sources producing a bubble with radius  $\bar{R}$ . Using Eqs. (20) and (21) we can Taylor expand  $\langle x_e \rangle$  around

small overdensities, to find

$$\begin{aligned} \langle x_e \rangle &= 1 - e^{\ln(1-\bar{x}_e)(1+b\delta_W)} \\ &\simeq 1 - (1 - \bar{x}_e) [1 + b\delta_W \ln(1 - \bar{x}_e)] + \mathcal{O}(\delta_W^2) \end{aligned} \quad (28)$$

Taking the Fourier transform of  $\xi_{xx}$  and  $\xi_{x\delta}$ , we obtain

$$P_{xx}^{2b}(k) = [\bar{x}_H \ln(\bar{x}_H) b \langle W_R \rangle(k)]^2 P_{\delta\delta}(k) \quad (29)$$

$$P_{x\delta}^{2b}(k) = \bar{x}_H \ln(\bar{x}_H) b \langle W_R \rangle(k) P_{\delta\delta}(k), \quad (30)$$

Note that here we are considering correlations of the neutral hydrogen fraction (perturbing the free electron fraction accounts for a minus sign in Eq. (30)). The superscript “2b” denotes the 2-bubble contribution. Also, we assume that the baryon fluctuations (the gas) trace the dark matter fluctuations. The total 2-bubble contribution to the power spectrum of  $X\psi$  results in

$$\begin{aligned} P_{X\psi}^{2b}(k) &\approx -\bar{x}_H^2 [\ln \bar{x}_H b \langle W_R \rangle(k) + 1]^2 P_{\delta\delta}(k) + \\ &\quad \bar{x}_H [\ln \bar{x}_H b \langle W_R \rangle(k) + 1] P_{\delta\delta}(k) \end{aligned} \quad (31)$$

As foreseen, the 2-bubble term is proportional to the total matter power spectrum with a scale dependent effective bias  $b_{\text{eff}}$ . When the universe is neutral,  $\bar{x}_H \rightarrow 1$ , the cross-correlation vanishes,  $P_{X\psi}^{2b}(k) = (-\bar{x}_H^2 + \bar{x}_H) P_{\delta\delta}(k) \rightarrow 0$ , while for  $\bar{x}_H \rightarrow 0$  all bubbles have merged and  $P_{X\psi}^{2b} \rightarrow 0$ .

Let us further investigate the behavior of the 2-bubble contribution. We can write  $P_{X\psi}^{2b}(k) = Q(1 - Q) P_{\delta\delta}(k) \equiv b_{\text{eff}} P_{\delta\delta}(k)$ , with  $Q(k, z) = \bar{x}_H \ln \bar{x}_H b \langle W_R \rangle + \bar{x}_H$ . We can distinguish two limiting cases: for  $Q > 1$  the power spectrum effective bias  $b_{\text{eff}}$  is negative, representing an anti-correlation, while for  $Q < 1$ ,  $b_{\text{eff}}$  is positive, and the 2-bubble term is positively correlated. In Fig. 2 we show  $b_{\text{eff}}$  for various values of the bubble bias  $b$  at  $z = 12$ . As reionization begins and ends, the 2-bubble term follows the matter power spectrum up to a scale-independent factor. The transition is around  $k\bar{R} \simeq 1$ , i.e. when the co-moving wavelength is similar to the average bubble size.

In the large scale limit, when  $k\bar{R} \ll 1$ ,  $b_{\text{eff}} \rightarrow \bar{x}_H (b \ln \bar{x}_H + 1) (\bar{x}_e - b \ln \bar{x}_H)$ . This function changes sign when  $\bar{x}_H > e^{-1/b}$ . In other words, the correlation function changes sign at large scales and at early times when the bias  $b$  also changes, as expected. In a merging scenario, the bubble radii are small at early times and this should give a smaller bias. Early on, when  $\bar{x}_H \sim 1$ , the large scales are always positively correlated, because even if the Universe contains relatively large bubbles, the fluctuations in the ionization fraction are small compared to the effectively homogeneous neutral fraction, and the 2-bubble term traces the matter power spectrum up to a scale-independent factor.

At scales that are smaller than the radius of the bubbles, the 2-bubble term is ill-defined: the correlation length becomes shorter than the size of the bubbles, effectively rendering them to one bubble. Therefore, we

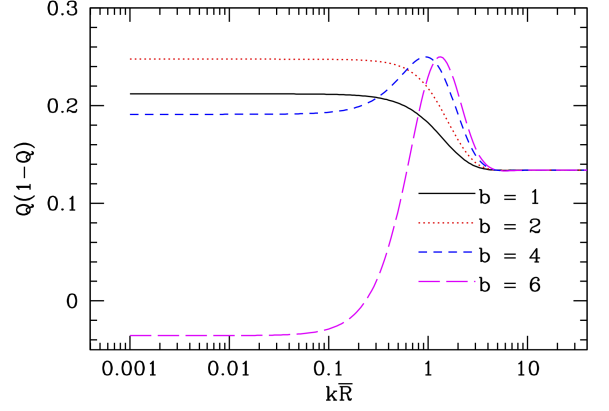


FIG. 2: The effective bias  $b_{\text{eff}} = Q(1 - Q)$  at  $z = 12$  as a function of  $k\bar{R}$ , where  $Q = \bar{x}_H \ln \bar{x}_H b \langle W_R \rangle + \bar{x}_H$  and  $P_{X\psi}^{2b}(k) = b_{\text{eff}} P_{\delta\delta}(k)$ . The sign of the large scale correlation function is set by the bias (and the value of  $\bar{x}_H$ ). A measurement of a positive correlation at high redshift would correspond to a small bubble bias. As reionization proceeds, and  $\bar{x}_H \rightarrow 0$ ,  $P_{X\psi}^{2b}$  becomes anti-correlated on large scales.

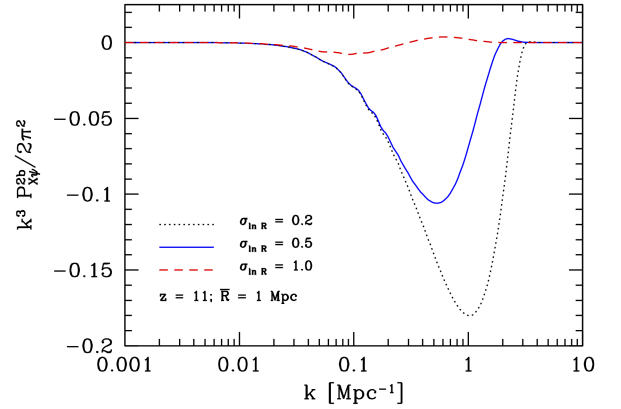


FIG. 3: The 2-bubble term or  $\bar{R} = 1$  Mpc, a bubble bias  $b = 6$ , and different values of the width of the log-normal distribution. The relative contribution of the 2-bubble term to the total correlation increases rapidly with decreasing  $\bar{R}$  and  $\sigma_{\ln R}$ , as derived in the Appendix.

will neglect the 2-bubble correlation term at those scales. In practice, we apply a smoothing filter that effectively cuts the correlation for  $kR_0 < 3$ . We show the 2-bubble contribution to the cross-correlation in Fig. 3.

## V. ONE BUBBLE CORRELATIONS

For scales much smaller than the average bubble radius, the correlation is dominated by the presence (or absence) of a single bubble [29]. The correlation between two (ionized) points separated by  $x_{12} = |\vec{x}_1 - \vec{x}_2|$  can be

written as [8, 9]

$$\langle x_e(\vec{x}_1)x_e(\vec{x}_2) \rangle = \bar{x}_e^2 + (\bar{x}_e - \bar{x}_e^2)f(x_{12}/R), \quad (32)$$

where  $f(x)$  is a function with the following limits:  $f(x) \rightarrow 1$  for  $x \ll 1$  and  $f(x) \rightarrow 0$  for  $x \gg 1$ . If the probability for finding one point inside an ionized bubble is  $\bar{x}_e$ , then when  $x_{12} \ll R$  the probability of finding the second point in the same bubble is 1, hence their joint correlation probability is  $\bar{x}_e$ . For large separations, the probability of finding two points in separate bubbles is the product of both probabilities, i.e.,  $\bar{x}_e^2$ . Eq. (32) effectively encodes the smooth transition between these two regimes. The 1-bubble correlation for free electrons (or equivalently neutral hydrogen) then becomes:

$$\xi_{xx_e}^{1b} = \langle x_e(\vec{x}_1)x_e(\vec{x}_2) \rangle - \bar{x}_e^2 = (\bar{x}_e - \bar{x}_e^2)f(x_{12}/R) \quad (33)$$

As long as the bubbles do not overlap, the function  $f$  can be described by the convolution of two top hat window functions  $\langle W_R^2 \rangle$ . The 1-bubble contribution to the power spectrum can then be written as

$$P_{X\psi}^{1b} = -(\bar{x}_e - \bar{x}_e^2) \left[ \langle V_b \rangle \langle W_R^2 \rangle(k) + \tilde{P}_{\delta\delta}(k) \right], \quad (34)$$

where

$$\tilde{P}_{\delta\delta}(k) = \langle V_b \rangle \int \frac{d^3k'}{(2\pi)^3} \langle W_R^2 \rangle(k') P_{\delta\delta}(|\vec{k} - \vec{k}'|) \quad (35)$$

The first term in Eq. (34) is the shot noise of the bubbles, which is a direct consequence of randomly placing ionizing galaxies in the Universe. We will later see that this term typically dominates the total correlation function at late times. This can be understood by realizing that the bubbles tend to be larger at late times, assuming that the bubble size increases over time through bubble merging.

Note that when correlating the free electrons with the neutral hydrogen, the 1-bubble contribution is always negative, i.e. these are fully anti-correlated when considering just single bubbles in the Universe. In the previous section we have also shown that the 2-bubble cross-correlation can be positive on the largest scales if the bubble bias is small. As reionization proceeds and the neutral hydrogen fraction decreases, the correlation on all scales will become anti-correlated. More importantly, the signal is proportional to the matter power spectrum, which grows as  $(1+z)^2$  during matter domination. The bubble bias is expected to grow as a function of the bubble radius and, therefore, we expect that any positive contribution to the correlation function would only appear at the earliest times, when the amplitude is suppressed.

It was shown by Ref. [29] that  $\tilde{P}_{\delta\delta}(k)$  can be approximated as

$$\tilde{P}_{\delta\delta}(k) \simeq \frac{P_{\delta\delta}(k) \langle V_b \rangle \langle \sigma_R^2 \rangle}{[(P_{\delta\delta}(k))^2 + (\langle V_b \rangle \langle \sigma_R^2 \rangle)^2]^{1/2}}, \quad (36)$$

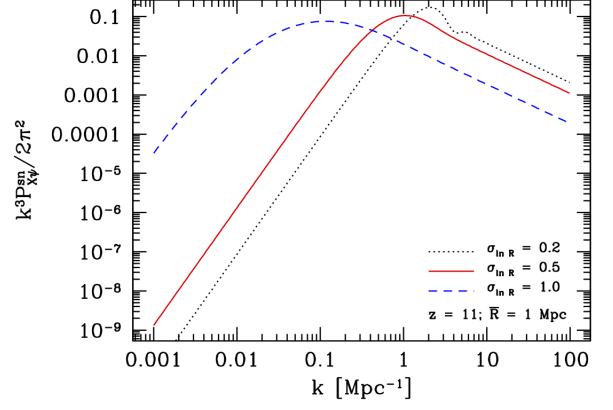


FIG. 4: The shot noise  $P_{X\psi}^{1b} \equiv (\bar{x}_e - \bar{x}_e^2) \langle V_b \rangle \langle W_R^2 \rangle$  for  $\bar{R} = 1$  Mpc and different values of the width of the log-normal distribution.

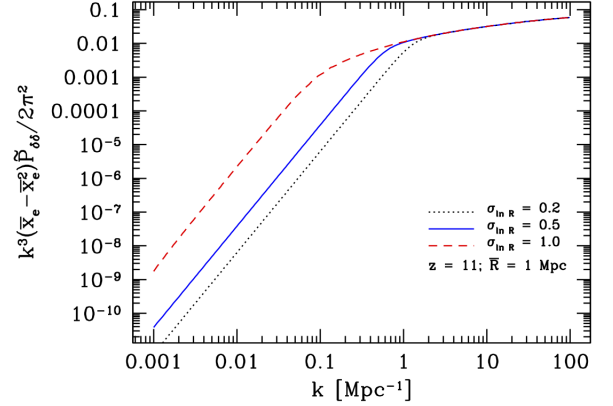


FIG. 5:  $\tilde{P}_{\delta\delta}$  as defined in the text for  $\bar{R} = 1$  Mpc and different values of the width of the log-normal distribution. This figure shows that this term is only relevant at small scales and does not contribute to the peak of the total correlation function.

which is derived by equating the small and large scale limits of Eq. (35) with

$$\langle \sigma_R^2 \rangle = \int \frac{k^2 dk}{2\pi^2} \langle W_R^2 \rangle(k) P_{\delta\delta}(k) \quad (37)$$

We have found the simple fitting solution of Eq. (36) to be accurate to the percent level for most values of  $\{\bar{R}, \sigma_{\ln R}\}$ . In the Appendix we will show that the contribution from  $\tilde{P}_{\delta\delta}(k)$  to the 1-bubble peak is relatively small for all parameter values in the range of interest for the  $\tau - 21$  cm cross-correlation, but is non-negligible and relevant at small scales.

We show the shot noise and  $\tilde{P}_{\delta\delta}$  in Figs. 4 and 5. The sum of these terms gives the 1-bubble power spectrum shown in Fig. 6. Note that the 1-bubble term from all three possible correlations ( $XX$ ,  $\psi\psi$  and  $X\psi$ ) is equivalent up to a sign.

In the small scale limit,  $\tilde{P}_{\delta\delta}(k) = P_{\delta\delta}(k)$ , and the 1-

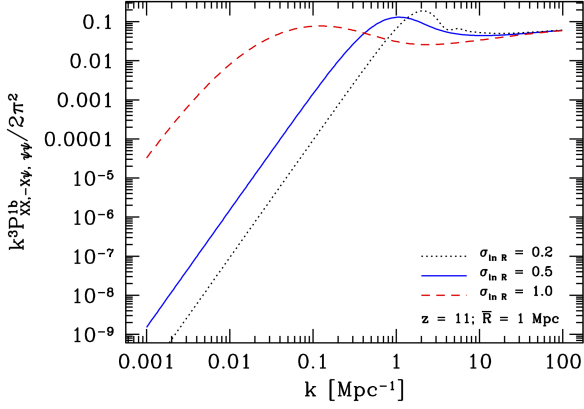


FIG. 6: The 1-bubble term for  $\bar{R} = 1$  Mpc and different values of the width of the log-normal distribution. The 1-bubble term has the same shape for correlations  $XX$ ,  $X\psi$  and  $\psi\psi$ .

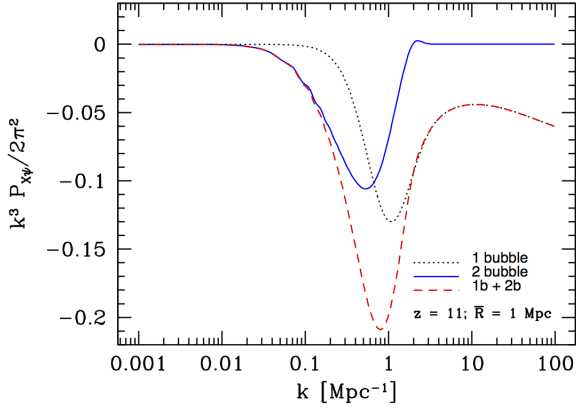


FIG. 7:  $k^3 P_{X\psi}(k)/2\pi^2$  for  $\bar{R} = 1$  Mpc,  $b = 6$  and  $\sigma_{ln R} = 0.5$ .

bubble term becomes:  $P_{X\psi}^{1b}(k) = -(\bar{x}_H - \bar{x}_H^2)P_{\delta\delta}(k)$ , rendering the total cross-correlation negative at these scales (at these scales we are applying a smoothing filter to the 2-bubble term, so it effectively does not contribute to the total cross-correlation). In Fig. 7 we show the total cross-correlation for  $\bar{R} = 1$  Mpc and  $\sigma_{ln R} = 0.5$  at  $z = 11$  (changing the redshift of the cross-correlation will predominantly affect the average ionization fraction  $\bar{x}_e$ ).

## VI. PROJECTED CROSS-CORRELATION

Fourier transforming the dimensionless brightness temperature  $\psi$ , we can write the spherical harmonic coefficient for the 21 cm fluctuation as

$$a_{\ell m}^{21} = 4\pi(-i)^\ell \int \frac{d^3 k}{(2\pi)^3} \hat{\psi}(\vec{k}) \alpha_\ell^{21}(k, z) Y_{\ell m}^*(\hat{k}), \quad (38)$$

where

$$\alpha_\ell^{21}(k, z) = T_0(z) \int_0^\infty d\chi' W_{\chi(z)}(\chi') j_\ell(k\chi') \quad (39)$$

Note that the response function is centered around  $\chi(z) = \chi'$ , and in practice we take this distance to be somewhere between  $z = 0$  and  $z = 30$ .

We can do the same for the optical depth to reionization, i.e. :

$$\tau_{\ell m} = 4\pi(-i)^\ell \int \frac{d^3 k}{(2\pi)^3} X(\vec{k}) \alpha_\ell^\tau(k) Y_{\ell m}^*(\hat{k}), \quad (40)$$

with

$$\alpha_\ell^\tau(k) = (1 - Y_p) \sigma_T \frac{\rho_{b,0}}{m_p} \int_0^{\chi_*} \frac{d\chi'}{a^2} j_\ell(k\chi'), \quad (41)$$

where  $\chi_*$  corresponds to the distance to last scattering.

Cross-correlating the two maps yields

$$\begin{aligned} \langle \tau_{\ell m} a_{\ell' m'}^{21*}(z) \rangle &= \delta_{\ell\ell'} \delta_{mm'} C_\ell^{\tau, 21}(z) \\ &= \int \frac{dk}{k} \Delta_{X\psi}^2(k) \alpha_\ell^\tau(k) \alpha_{\ell'}^{21}(k, z) \end{aligned} \quad (42)$$

Here,  $\Delta_{X\psi}^2 = k^3 P_{X\psi}/(2\pi^2)$ .

Let us consider the cross-correlation in the Limber approximation. Under this approximation, we can assume that the Bessel functions are small,  $j_\ell(x) \ll 1$ , for  $x < \ell$  and peak when  $x \sim \ell$ . The integral over comoving momentum  $k$  will get most of its contribution from modes  $k \sim \ell/\chi$ . Therefore we can make the approximation that  $\Delta_{X\psi}^2(k) \sim \Delta_{X\psi}^2(\ell/\chi)$  and re-write Eq. (42) as

$$\begin{aligned} C_\ell^{\tau, 21}(z) &= (1 - Y_p) \frac{T_0(z) \rho_{b,0} \sigma_T}{m_p} \\ &\int_0^{z_*} \frac{dz'_1}{H(z'_1)} (1 + z'_1)^2 \int_0^\infty \frac{dz'_1}{H(z'_1)} W_z(\chi(z'_1)) \\ &\times 4\pi \int \frac{dk}{k} \Delta_{X\psi}^2(k) j_\ell(k\chi(z'_1)) j_\ell(k\chi(z'_2)) \end{aligned} \quad (43)$$

Again, in practice we take the window function to be centered around  $0 \leq z \leq 30$ .

In the Limber approximation we can perform the  $k$  integral over the product of Bessel functions as:

$$\int_0^\infty dk k^2 j_\ell(k\chi(z_1)) j_\ell(k\chi(z_2)) = \frac{\pi}{2} \frac{\delta(\chi(z_1) - \chi(z_2))}{\chi^2} \quad (44)$$

Thus, we can write the angular cross spectrum as

$$\begin{aligned} C_\ell^{\tau, 21}(z) &= (1 - Y_p) \frac{T_0(z) \rho_{b,0} \sigma_T}{m_p} \int_0^\infty dz' \frac{W_z(\chi(z'))}{H^2} \\ &\times \left| \frac{d\chi}{dz} \right|^{-1} \left( \frac{1 + z'}{\chi(z')} \right)^2 P_{X\psi} \left( \frac{\ell}{\chi(z')}, z' \right) \end{aligned} \quad (45)$$

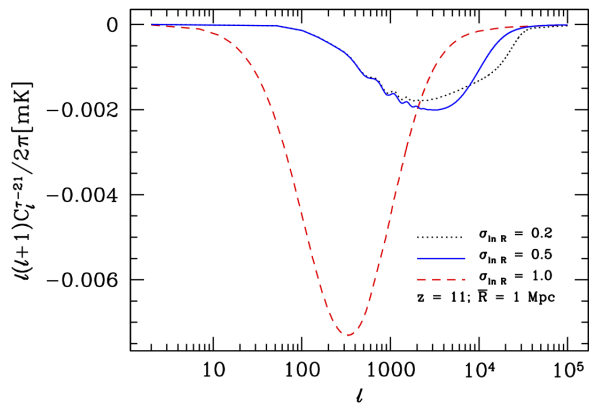


FIG. 8: The cross-correlation between 21 cm temperature brightness fluctuations and the optical depth  $\tau$  at  $z = 11$  for a model with  $\bar{R} = 1$  Mpc and  $b = 6$ . Here we used a Gaussian window function with bandwidth frequency  $\Delta\nu = 0.2$  MHz.

We will assume that the window function is a Gaussian centered around redshift  $z$  with width  $\delta\chi$  given by

$$\delta\chi \simeq \left( \frac{\Delta\nu}{0.1\text{MHz}} \right) \left( \frac{1+z}{10} \right)^{1/2} \left( \frac{\Omega_m h^2}{0.15} \right)^{-1/2} \text{Mpc} \quad (46)$$

where  $\Delta\nu$  is the bandwidth frequency of the instrument. We have taken into account that the power spectrum explicitly depends on redshift.

We show the angular cross-correlation for  $\Delta\nu = 0.2$  MHz and several values of  $\sigma_{\ln R}$  in Fig. 8.

In the previous sections we have shown that the cross-correlation between free electrons and neutral hydrogen has a strong dependence on the parameters that determine the bubble distribution as well as its bias. The location of the peak is set by an effective scale, which we derive in the Appendix. We will see that for a log-normal bubble distribution, this effective scale is exponential in the width of the distribution and inversely proportional to the average bubble radius. Therefore, a small change in the width of the distribution can produce a large change in the location of the peak. We have also shown that at early times the 2-bubble term can be positively correlated at large scales. The positive contribution to the correlation function at large scales eventually vanishes when the universe further reionizes. However, if the bubbles are small enough, a positive contribution to the correlation function could persist until late times. Oppositely, if bubbles are relatively large (a few Mpc), the shot noise, which is negative for all scales, will dominate the correlation function.

## VII. IS THE CROSS-CORRELATION DETECTABLE?

### A. Signal-to-noise

In this section we will determine if the cross-correlation is detectable. An important issue that we will address here are the foregrounds. As previously mentioned, the 21 cm emission should be swamped by foregrounds, dominated by polarized Galactic synchrotron, a signal that is at least 4 orders of magnitude larger than the 21 cm brightness. We do not know the spectral dependence of all these foregrounds, but in general we can assume that they are relatively smooth in frequency along the line of sight, since they typically come from the same source (e.g. our own Galaxy). In principle, one can therefore remove a large part of the foregrounds by removing the largest modes along the line of sight (see e.g. [33] for a recent discussion).

However, when cross-correlating the 21 cm field with the optical depth, we want to keep the largest modes, to which the integrated optical depth is most sensitive. Hence, we will keep the foregrounds in the observed maps and show that the cross-correlation between foregrounds in the 21 cm field and in the CMB should be small. In order to neglect the cross-correlation of the foregrounds between  $\tau$  and 21 cm, we typically need the foreground of the CMB to be  $\leq 10^{-5}$  times the signal [27] (given that  $a_{\ell m}^{f,21} \sim 10^5 a_{\ell m}^{21}$ ). The synchrotron emission is roughly equal to the CMB signal at 1 GHz. Therefore, if we assume that the synchrotron scales as  $\nu^{-3}$  [34], at 94 GHz (W band) we have  $a_{\ell m}^{\text{synchrotron}} \sim \times 10^{-6} a_{\ell m}^{\text{CMB}}$ . Thus, we estimate that the signal will be larger than the remaining foregrounds after cross-correlating the two maps.

Additionally, by not removing the foregrounds, the 21cm foregrounds will effectively act as noise term in the cross-correlation. In other words, even in the absence of correlation between foregrounds, there is still a finite probability that any given data point in the  $\tau$  map will correlate with a foreground measurement from 21 cm, i.e. the induced noise contains a term  $\langle \tau_{\ell m} a_{\ell' m'}^{f,21} \rangle$ , where the latter is the spherical harmonic coefficient of the 21 cm foreground map.

Unfortunately, we do not know exactly what the level of synchrotron foreground is, but typically  $C_{\ell}^f \sim k\ell^{-\alpha}$ , with  $2 < \alpha < 4$ . We will assume that the synchrotron emission scales as  $\nu^{-3}$ . In Ref. [35] it was shown that synchrotron emission at 480 MHz has a normalized amplitude of  $100 \text{ mK}^2 < C_{\ell=100}^f < 10000 \text{ mK}^2$ , with the actual amplitude and slope depending on the position in the sky.

Although we cannot remove the foregrounds through implementing a large scale cutoff, we can alternatively try to remove a substantial part of galactic foreground emission. If there is a large correlation between different frequencies of the foreground maps, one could measure the foregrounds at high frequency (corresponding to a

completely ionized universe and, hence, with no signal in the cross-correlation), extrapolate with an appropriate scaling  $\sim \nu^{-3}$  and subtract those from the high redshift maps. If the correlation between different maps at high frequencies is of order  $0.9 - 0.99$ , one could reduce the overall amplitude of the foreground by a factor of  $10 - 100$  and the power by a factor of a  $100 - 10^4$ <sup>1</sup>. In addition, in Ref. [28] it was shown that down weighting the most heavily contaminated regions in the sky can reduce the effective foreground as much as a factor of 2. Note that this approach is different from the usual spectral fitting techniques [6, 36–38].

We will consider a case in which the angular power spectrum of the foreground is given by:

$$C_\ell^f(z) \simeq \frac{10^6}{2} \frac{1}{c_f} \text{mK}^2 \ell^{-3} \left( \frac{f(z)}{480 \text{ MHz}} \right)^{-3}, \quad (47)$$

where  $f(z)$  corresponds to the frequency of the redshift considered and  $100 \leq c_f \leq 10^4$  is the foreground reduction factor that we can hope to achieve through a measurement at low redshift.

We will assume a noise power spectrum given by [6, 15, 39, 40],

$$N_\ell^{21,21} = \frac{2\pi}{\ell^2} (20 \text{ mK})^2 \left[ \frac{10^4 \text{ m}^2}{A_{\text{eff}}} \right]^2 \left[ \frac{10'}{\Delta\Theta} \right]^4 \left[ \frac{1+z}{10} \right]^{9.2} \times \left[ \frac{\text{MHz}}{\Delta\nu} \frac{100 \text{ hr}}{t_{\text{int}}} \right] \quad (48)$$

We will do forecasts for a total integration time of 1000 hours, and a beam with an angular diameter of  $\Delta\Theta = 9$  arcmin. We set the bandwidth to  $\Delta\nu = 0.2$  MHz. For a LOFAR type experiment, we use  $A_{\text{eff}} = 10^4 \text{ m}^2$  and for a Square Kilometer Array (SKA) type experiment we use  $A_{\text{eff}} = 10^5 \text{ m}^2$ .

On the CMB side, experiments are rapidly improving [41–44], with high sensitivity experiments coming soon (Planck, ACTPol, SPTPol, CMBPol) and we should have observations of the E- and B-modes polarization spectra up to small scales in the near future. We will now consider a next generation polarization experiment that allows us to reconstruct a map of the optical depth  $\tau_{\ell m}$  with the estimator proposed by Ref. [21]. This estimator was built to extract the inhomogeneous reionization signal from future high-sensitivity measurements of the cosmic microwave background temperature and polarization fields. The authors in Ref. [21] wrote a minimum variance quadratic estimator for the modes of the optical depth field given by:

$$\hat{\tau}_{\ell m} = N_\ell^{\tau\tau} \sum_{\ell_1 m_1 \ell_2 m_2} \Gamma_{\ell_1 \ell_2 \ell}^{EB} \begin{pmatrix} \ell_1 & \ell_2 & \ell \\ m_1 & m_2 & m \end{pmatrix} \times \frac{a_{\ell_1 m_1}^{E*} a_{\ell_2 m_2}^{B*}}{(C_{\ell_1}^{EE} + N_{\ell_1}^{EE})(C_{\ell_2}^{BB} + N_{\ell_2}^{BB})}, \quad (49)$$

where  $C_\ell^{EE}$  and  $C_\ell^{BB}$  are the E- and B-mode polarization power spectra.  $N_\ell^{EE}$  and  $N_\ell^{BB}$  correspond to the CMB noise power spectra, and are given by:

$$N_\ell^{EE} = N_\ell^{BB} = \Delta_P^2 \exp\left(\frac{\ell(\ell+1)\theta_{\text{FWHM}}^2}{8 \ln(2)}\right), \quad (50)$$

where  $\Delta_P$  is the detector noise and  $\theta_{\text{FWHM}}$  is the beam size.

The coupling  $\Gamma_{\ell_1 \ell_2 \ell}^{EB}$  can be written as

$$\Gamma_{\ell_1 \ell_2 \ell}^{EB} = \frac{C_{\ell_1}^{E_0 E_1}}{2i} \sqrt{\frac{(2\ell_1+1)(2\ell_2+1)(2\ell+1)}{4\pi}} \times \left[ \begin{pmatrix} \ell_1 & \ell_2 & \ell \\ -2 & 2 & 0 \end{pmatrix} - \begin{pmatrix} \ell_1 & \ell_2 & \ell \\ 2 & -2 & 0 \end{pmatrix} \right] \quad (51)$$

Here  $C_{\ell_1}^{E_0 E_1}$  is the cross-power spectrum between the CMB  $E_0$ -mode polarization without patchy reionization and the response field to  $\tau$  fluctuations  $E_1$ . ( $C_{\ell}^{E_0 E_1}$  is positive at large scales due to Thomson scattering, and negative at small scales due to the screening).

Furthermore, the reconstruction noise power spectrum is given by:

$$N_\ell^{\tau\tau} = \left[ \frac{1}{2\ell+1} \sum_{\ell_1 \ell_2} \frac{|\Gamma_{\ell_1 \ell_2 \ell}^{EB}|^2}{(C_{\ell_1}^{EE} + N_{\ell_1}^{EE})(C_{\ell_2}^{BB} + N_{\ell_2}^{BB})} \right]^{-1} \quad (52)$$

We note that the main source of contamination in reconstructing  $\tau(\hat{n})$  comes from the non-Gaussian signal from gravitational lensing of the CMB. In principle, unbiased estimators that simultaneously reconstruct the inhomogeneous reionization signal and the gravitational potential can be constructed [45]. For purposes of simplicity, we will estimate our cross-correlation using the estimator given by Eq. (49), but the results in this work are straightforward to generalize.

Given that the  $\tau$  map is not sensitive to redshift (Ref. [21] showed that the estimator is only sensitive to one principal component in redshift), while the 21 cm map can be reconstructed on redshift slices, we will give a weight to the cross-correlation. This weight will be built in order to maximize the signal to noise, in the same spirit as in Ref. [46], where a weight was derived for the cross-correlations between CMB and Galaxy surveys. We write the weighted 21 cm maps as

$$\tilde{a}_{\ell m}^{21}(z) = \int_0^z dz' a_{\ell m}^{21}(z') w_\ell(z') \quad (53)$$

<sup>1</sup> Note that this is a very crude estimate. For example, it might be relevant to consider 21 cm signals after reionization (at low  $z$ ) due to residual neutral hydrogen, primarily in Damped Ly $\alpha$  absorbers (DLA's).

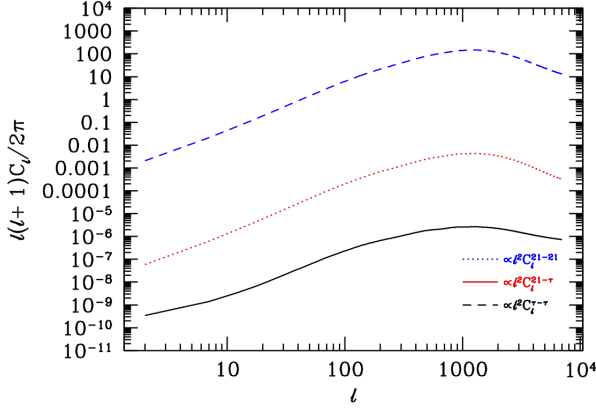


FIG. 9: The different power spectra used to compute the signal to noise in Fig. 10. The sign of  $C_\ell^{21-\tau}$  has been inverted for the sake of comparison. The spectra are shown at  $z = 11$ .

We then want to maximize

$$\chi_{\ell m}^2 = \frac{\langle \tau_{\ell m}^* \tilde{a}_{\ell m}^{21}(z) \rangle^2}{\langle \tau_{\ell m} \tau_{\ell m}^* \rangle \langle \tilde{a}_{\ell m}^{21}(z) \tilde{a}_{\ell m}^{21*}(z) \rangle}, \quad (54)$$

and, in doing so, we find:

$$w_\ell(z) = \frac{C_\ell^{\tau,21}(z)}{(C_\ell^{21,21} + N_\ell^{21,21} + C_\ell^f)(z)}, \quad (55)$$

which is nothing else then the projected signal over the projected noise. Note that we have included the foreground as a source of noise as explained before.

We can now compute the signal to noise for the  $\tau$ -21 cm cross-correlation as

$$\left(\frac{S}{N}\right)^2 = f_{\text{sky}} \sum_\ell (2\ell + 1) \times \int dz \frac{|C_\ell^{\tau,21}(z)|^2}{(C_\ell^{\tau,\tau} + N_\ell^{\tau\tau})(C_\ell^{21,21} + N_\ell^{21,21} + C_\ell^f)(z)} \quad (56)$$

In Fig. 10 we assess the level of detectability for a model with  $\bar{R} = 5$  Mpc and  $\sigma_{\ln R} = 0.5$  (see Fig. 9 for the angular spectra of the model considered). Again, to generate the spectra we use a Gaussian window function with  $\Delta\nu = 0.2$  MHz. We find that the signal to noise reaches  $f_{\text{sky}}^{-1/2} S/N = 8$  at  $\ell_{\text{max}} = 3000$  for a LOFAR type experiment, while for a SKA type experiment it reaches  $f_{\text{sky}}^{-1/2} S/N = 26$ , with  $f_{\text{sky}}$  being the fraction of the sky covered. We note that for  $\ell_{\text{max}} \geq 1000$ , the signal to noise does not vary substantially when considering different values of the parameter  $c_f$ , that represents the level of foreground subtraction.

## B. Reionization parameters

In this section we will assess what we can learn about reionization by studying the 21 cm- $\tau$  cross-correlation.

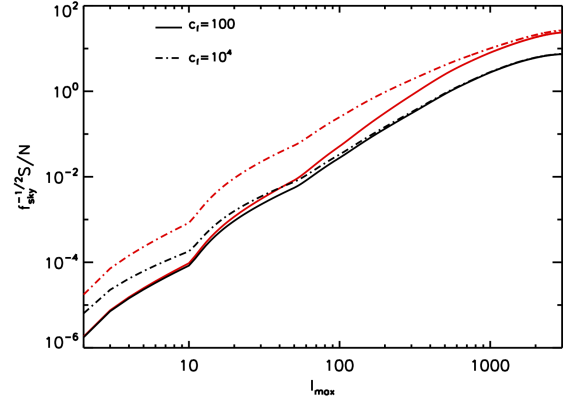


FIG. 10: Total signal-to-noise for the 21 cm- $\tau$  cross-correlation as a function of  $\ell_{\text{max}}$  for a model with  $\bar{R} = 5$  Mpc and  $\sigma_{\ln R} = 0.5$ . We consider an experiment with CMB noise power spectra given by  $\Delta_P = 0.3 \mu\text{K-arcmin}$  and beam size  $\Theta_{FWHM} = 1$  arcmin. The foreground angular power spectrum is given by Eq. (47). We show forecasts for a SKA type experiment (in red lines) and a LOFAR type experiment (in black lines). At  $\ell \geq 1000$ , the signal-to-noise does not vary substantially when considering different values of the parameter  $c_f$ , which represents the level of foreground subtraction.

We will forecast parameter uncertainties in the following parameters  $\pi = \{\bar{R}, \sigma_{\ln R}, b, \tau, \Delta y\}$ .

As a forecasting tool we will use a Fisher matrix analysis, where the Fisher matrix is given by [47]:

$$F_{\mu\nu} = f_{\text{sky}} \sum_\ell (2\ell + 1) \times \int dz \frac{(\partial C_\ell^{\tau,21}(z)/\partial \pi_\mu)(\partial C_\ell^{\tau,21}(z)/\partial \pi_\nu)}{(C_\ell^{\tau,\tau} + N_\ell^{\tau\tau})(C_\ell^{21,21} + N_\ell^{21,21} + C_\ell^f)(z)} \quad (57)$$

where  $\mu$  and  $\nu$  run over the parameter modes.

The rms uncertainty on the parameter  $\pi_\mu$  is given by  $\sigma(\pi_\mu) = (F_{\mu\mu}^{-1})^{1/2}$  if the other parameters are marginalized. If the remaining parameters are assumed fixed, then the rms is  $\sigma(\pi_\mu) = (F_{\mu\mu})^{-1/2}$ .

We consider a next generation polarization experiment with noise power spectrum given by  $\Delta_P = 0.3 \mu\text{K-arcmin}$  and beam size  $\Theta_{FWHM} = 1$  arcmin.

When assuming a LOFAR type experiment, the bias can be constrained at the 33% level,  $\bar{R}$  at the 20% level,  $\sigma_{\ln R}$  at the 11% level,  $\Delta y$  at the 15% level, and  $\tau$  at the 6% level, when the remained parameters are fixed. With a SKA type experiment, the bias can be constrained at the 11% level,  $\bar{R}$  can be constrained at the 6% level,  $\sigma_{\ln R}$  at the 3% level,  $\Delta y$  at the 5% level, and  $\tau$  at the 2% level, when the remaining parameters are considered fixed.

We show the error ellipses for the optical depth, the bias and the width of reionization in Figs. 11 and 12. The Planck priors are shown in dashed lines. For a LOFAR level of noise, and an experiment that measures the

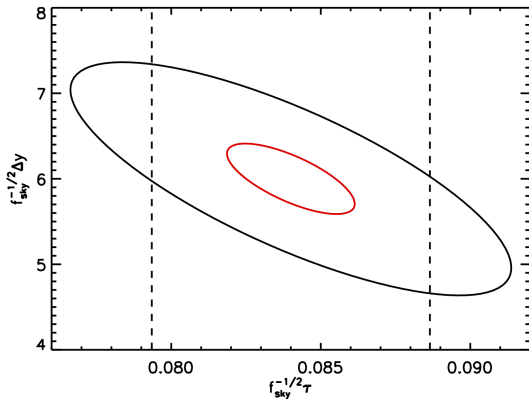


FIG. 11: Forecasted uncertainties on the width of reionization parameter  $\Delta y$  and the optical depth  $\tau$  (assuming that the other parameters are fixed) for a LOFAR type experiment (in black lines) and a SKA type experiment (in red lines). For reference, the dashed lines correspond to the Planck priors on the optical depth.

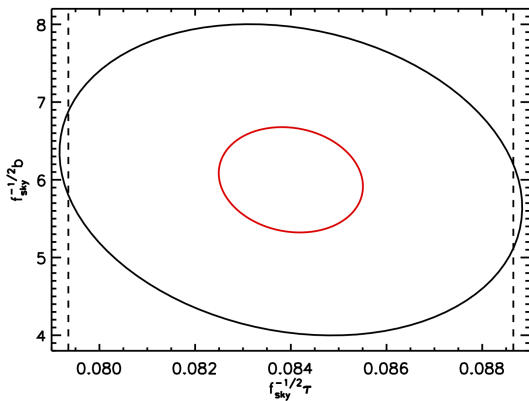


FIG. 12: Forecasted uncertainties on the bubble bias  $b$  and the optical depth  $\tau$  (assuming that the other parameters are fixed) for a LOFAR type experiment (in black lines) and a SKA type experiment (in red lines). For reference, the dashed lines correspond to the Planck priors on the optical depth.

full sky, the constraints on the optical depth are comparable to the expected ones from Planck. For a SKA type experiment, the constraints shrink by a factor of  $\sim 3$ .

### VIII. DISCUSSION AND CONCLUSION

We investigated the correlation between free electrons, traced by the optical depth  $\tau$ , and neutral hydrogen, traced through the emission of 21 cm photons, during the epoch of reionization. To compute the cross-correlation we used a simple model where patches of ionized gas are represented by spherical bubbles. The cross-correlation

will depend on the presence or absence of these bubbles (the 1-bubble term) and the clustering of bubbles (the 2-bubble term). As expected, the cross-correlation is negative on small scales, where it is dominated by the shot noise of the bubbles. On large scales, the 2-bubble term can render the correlation positive as long as the effective bias  $b_{\text{eff}}$  is large. Small bubbles at a fixed neutral hydrogen fraction imply a small bubble bias, hence the 2-bubble term has a suppressed (positive) amplitude. A larger correlation could be driven by the ionization fraction, but within a bubble merger scenario the smallest bubbles are expected at early times, when the ionization fraction is small and the total matter power spectrum is suppressed.

The anti-correlation peak, set by the sum of the 1-and the 2-bubble terms, depends critically on the distribution of the ionized bubbles. Consequently, a measurement of the cross-correlation allows us to probe the parameters relevant for the reionization history. In principle a measurement of a positive correlation at early times, could set fairly stringent constraints on the bubble size and the bubble bias, providing a complementary probe into these EoR parameters.

One major obstacle in measuring the 21 cm emission from the EoR are the large foregrounds at these frequencies. For the auto-correlation, any detection requires a careful removal of foregrounds, which typically results in the removal of the largest modes along the line of sight. The advantage of the cross-correlation is that foregrounds in the measurement of  $\tau$  are weakly correlated with those in the 21 cm field. Therefore, the cross-correlation is less sensitive to the detailed understanding of the foregrounds.

In this paper we have computed the signal to noise of the cross-correlation using the estimator for inhomogeneous reionization  $\hat{\tau}_{\ell m}$  proposed by Ref. [21]. In our computation there is very little contribution from any positive correlation at large scales coming from 2-bubble term, and most of the signal comes from the shot noise. Because a measurement of the optical depth gets most of its signal from the long wavelength mode along the line of sight, we left the 21 cm foregrounds as a noise term. Although the signal to noise per mode is small, the large number of modes allows for a detection when considering a next generation 21 cm experiment cross-correlated with a CMB experiment that measures the polarization  $B$ -modes in most of the sky. We expect that around the time SKA observes a large part of the sky, CMB experiments will have improved to the level that we are able to reconstruct a map of  $\tau_{\ell m}$ . Although the auto-correlation of both maps will give significant insight into reionization, cross-correlating these maps will give a complementary probe. We find that a measurement of this cross-correlation with a detector noise level of a LOFAR type experiment on the 21 cm side and noise level of a next generation polarization type experiment on the CMB side constrains the width of the ionization history at the 15% level, the bias parameter at the 33% level,

the bubble radius at the 20% level, and the width of the bubble distribution at the 11% level. The constraint on the optical depth (at the 6% level) is similar to what we expect to see with the Planck satellite. The previous results are considering that both experiment measure the full sky. If they measure part of the sky, the constraints will degrade as  $f_{\text{sky}}^{-1/2}$ . Finally, a SKA type experiment will be able to shrink these constraints by a factor of  $\sim 3$ .

### Acknowledgments

The authors would like to thank Renyue Cen, Enrico Pajer, Fabian Schmidt, Kendrick Smith, and Matias Zaldarriaga for useful discussions. P.D.M is supported by the Netherlands Organization for Scientific Research (NWO), through a Rubicon fellowship. C.D. is supported by the National Science Foundation grant number AST-0807444, NSF grant number PHY-0855425, and the Raymond and Beverly Sackler Funds. P.D.M. and D.N.S. are in part funded by the John Templeton Foundation grant number 37426.

### Appendix A: Dependence on $\bar{R}$ and $\sigma_{\ln R}$

The choice of a log-normal distribution is motivated in part by simulations by Refs. [32] and [29]. In this paper we have made the assumption that the distribution is static (i.e. that  $\bar{R}$ ,  $\sigma_{\ln R}$  and the distribution itself do not change in time). We have already seen that variations in  $\sigma_{\ln R}$  change both the location and the amplitude of the peak of the 21 cm- $\tau$  cross-correlation. In this section we will consider implications of varying EoR parameters with a log-normal and a normal bubble distribution on the 1-and-2-bubble terms. In particular, we will compare both contributions to the amplitude of the anti-correlation peak.

#### 1. Log-normal distribution

We first start by investigating the implications of a log-normal distribution for the bubble radius.

The bubble distribution is given by

$$P(R, \sigma_{\ln R}) = \frac{1}{\bar{R}} \frac{1}{\sqrt{2\pi\sigma_{\ln R}^2}} e^{-[\ln(R/\bar{R})]^2 / (2\sigma_{\ln R}^2)} \quad (\text{A1})$$

Given this distribution we can compute the average bubble size:

$$\langle V_b \rangle = \int dR P(R) V_b(R) = \frac{4\pi \bar{R}^3}{3} e^{9\sigma_{\ln R}^2 / 2} \quad (\text{A2})$$

To address the dependence of the resulting correlation function, we also need the variance

$$\langle V_b^2 \rangle = \int dR P(R) V_b^2(R) = \frac{(4\pi)^2 \bar{R}^6}{9} e^{18\sigma_{\ln R}^2} \quad (\text{A3})$$

The amplitude of the 1- and 2-bubble terms, and the relevant scale where these peak, strongly depend on the window function

$$W_R(k) = \frac{3}{(kR)^3} [\sin(kR) - kR \cos(kR)] \quad (\text{A4})$$

Recall the the volume averaged window function and window function squared (shown in Figs. 13 and 14) are defined as

$$\langle W_R \rangle(k) = \frac{1}{\langle V_b \rangle} \int_0^\infty dR P(R) V_b(R) W_R(kR), \quad (\text{A5})$$

and

$$\langle W_R^2 \rangle(k) = \frac{1}{\langle V_b \rangle^2} \int_0^\infty dR P(R) V_b^2(R) W_R^2(kR) \quad (\text{A6})$$

The total correlation function can be written as

$$P_{X\psi} = P_{X\psi}^{1b} + P_{X\psi}^{2b}, \quad (\text{A7})$$

where the 1-bubble contribution consists of two relevant terms: the shot noise and the power spectrum  $\tilde{P}_{\delta\delta}$  given by Eq. (36).

Let us define the following relevant ratios:

$$R^{2b-sn} \equiv P_{X\psi}^{2b} / P_{X\psi}^{sn} \quad (\text{A8})$$

and

$$R^{1b-sn} \equiv \tilde{P}_{\delta\delta} / P_{X\psi}^{sn}, \quad (\text{A9})$$

where  $P_{X\psi}^{sn}$  is the contribution from the shot noise, which is given by

$$P_{X\psi}^{sn} = -(\bar{x}_e - \bar{x}_e^2) \langle V_b \rangle \langle W_R^2 \rangle(k) \quad (\text{A10})$$

In the limit of small comoving momenta (large scales),  $\langle W_R \rangle \rightarrow 1$ , and  $\langle W_R^2 \rangle \rightarrow \langle V_b^2 \rangle / \langle V_b \rangle^2$ .

For small scales, we have:

$$\begin{aligned} \langle W_R^2 \rangle(k, \bar{R}, \sigma_{\ln R}) &\sim \frac{9}{2k^4 \langle V_b \rangle^2} \int_0^\infty \frac{dR}{R^4} P(R) V_b^2(R) \\ &= \frac{9}{2k^4 \bar{R}^4} e^{-7\sigma_{\ln R}^2} \end{aligned} \quad (\text{A11})$$

Roughly speaking, we know that the contribution from the shot noise term will be constant and have a peak at some characteristic scale after which it will decrease as  $\propto 1/k^4$ . Furthermore, up until that characteristic scale, the amplitude of the shot noise is boosted with respect to all the other terms as  $\langle V_b^2 \rangle / \langle V_b \rangle^2 = e^{9\sigma_{\ln R}^2}$ .

The characteristic scale is determined by equating the two limiting cases [48], i.e.

$$\frac{(4\pi)^2 \bar{R}^6}{9} e^{18\sigma_{\ln R}^2} = \frac{(4\pi)^2 \bar{R}^2}{2k^4} e^{2\sigma_{\ln R}^2}, \quad (\text{A12})$$

This tells us that the shot noise roughly peaks around

$$k_{peak} = \left( \frac{9}{2\bar{R}^4} e^{-16\sigma_{\ln R}^2} \right)^{1/4} \quad (\text{A13})$$

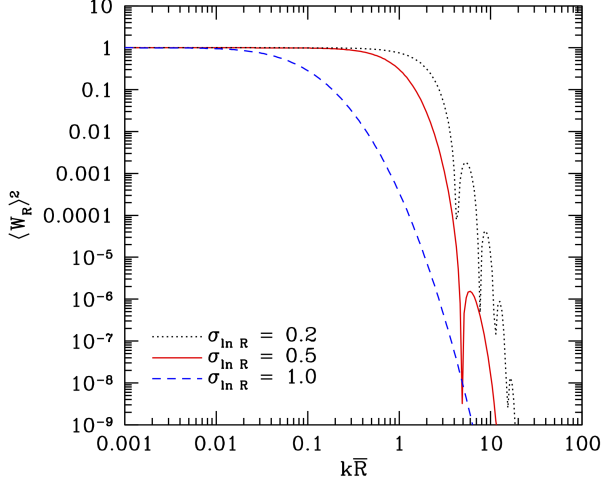


FIG. 13:  $\langle W_R \rangle^2$  for different values of  $\sigma_{\ln R}$ .

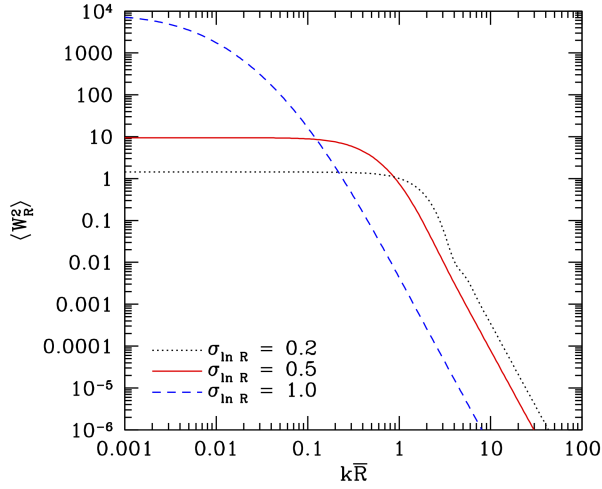


FIG. 14:  $\langle W_R^2 \rangle$  for different values of  $\sigma_{\ln R}$ . Note that the maximum amplitude in the limit  $k\bar{R} \ll 1$  grows exponentially in  $\sigma_{\ln R}$ , which will be relevant for the relative contribution of the shot noise with respect to the 1- and 2- bubble terms.

The second contribution to the 1-bubble term comes from  $\tilde{P}_{\delta\delta}(k)$ , which is given by

$$\tilde{P}_{\delta\delta}(k) = \langle V_b \rangle \int \frac{d^3 k'}{(2\pi)^3} \langle W_R^2 \rangle(k') P_{\delta\delta}(|\vec{k} - \vec{k}'|) \quad (\text{A14})$$

As it was shown in Ref. [29], in the large scale limit we have:

$$\lim_{k\bar{R} \ll 1} \tilde{P}_{\delta\delta}(k) \simeq \langle V_b \rangle \int_0^\infty \frac{dk}{2\pi^2} k^2 \langle W_R^2 \rangle(k) P_{\delta\delta}(k) \quad (\text{A15})$$

In this limit,  $\langle W_R^2 \rangle \rightarrow \langle V_b^2 \rangle / \langle V_b \rangle^2$ , which allows us to put the following constraint on the amplitude of  $\tilde{P}_{\delta\delta}(k)$

$$\tilde{P}_{\delta\delta} \lesssim \frac{\langle V_b^2 \rangle}{\langle V_b \rangle} \int_0^{k_{peak}} k^2 dk P_{\delta\delta}(k) \quad (\text{A16})$$

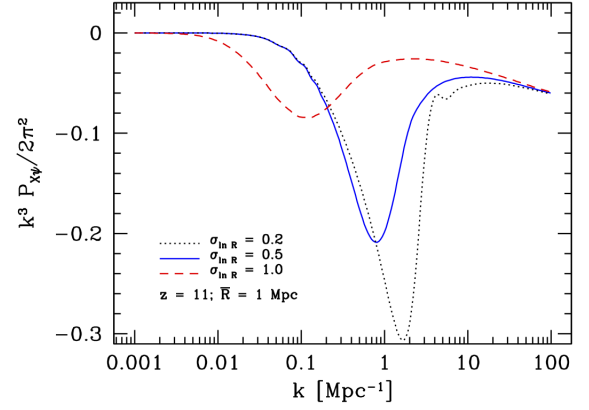


FIG. 15:  $k^3 P_{X\psi}(k) / 2\pi^2$  for  $\bar{R} = 1$  Mpc,  $b = 6$  at different values of  $\sigma_{\ln R}$ .

The relative peak amplitude between the two contributions in the 1-bubble term is therefore given by

$$R^{1b-sn} \equiv \tilde{P}_{\delta\delta} / P_{X\psi}^{sn} \lesssim \frac{1}{2\pi^2} \int_0^{k_{peak}} k^2 dk P_{\delta\delta}(k) \quad (\text{A17})$$

Since  $k_{peak}$  depends on the bubble radius and on  $\sigma_{\ln R}$ , so does the relative contribution. Generally speaking, a narrower distribution (with smaller  $R_0$ ) leads to a larger contribution from  $\tilde{P}_{\delta\delta}$  to the total 1-bubble term. That being said, even for very narrow distributions and very small average bubble radius we find that the total contribution to the peak does not exceed more than a few percent, i.e., in realistic scenarios the shot noise term dominates the total 1-bubble term (see e.g. Ref. [49]). In Fig. 15 we plot the cross-correlation  $X\psi$  for different values of  $\sigma_{\ln R}$ , confirming our estimate for the peak sale in Eq. (A13).

There is one caveat, which is that  $\tilde{P}_{\delta\delta}$  does not drop as fast as the shot noise, hence at small scales this term can contribute more. In fact, it is this term the responsible for the turnover at small scales of the  $\tau$ - $\tau$  and 21-21 auto power spectra (see Figs. 16 and 17).

We remind the reader that the 2-bubble contribution to the  $X\psi$  cross-correlation is given by:

$$P_{X\psi}^{2b} \approx -\bar{x}_H^2 [\ln \bar{x}_H b \langle W_R \rangle + 1]^2 P_{\delta\delta}(k) + \bar{x}_H [\ln \bar{x}_H b \langle W_R \rangle + 1] P_{\delta\delta}(k) \quad (\text{A18})$$

The minimum value  $P_{X\psi}^{2b}$  is reached when  $\bar{x}_H = e^{-1-1/b}$ , while for the shot noise term  $\bar{x}_e = 0.5$  represents the peak value. We can now compare the 2-bubble terms to the shot noise:

$$R^{2b-sn} \equiv P_{X\psi}^{2b} / P_{X\psi}^{sn} \lesssim \frac{16}{3\pi} b e^{-1-1/b} (1 + e^{-1-1/b}) \times P_{\delta\delta}(k_{peak}) e^{-27\sigma_{\ln R}/2} \quad (\text{A19})$$

When considering  $\bar{R} = 1$  Mpc and  $\sigma_{\ln R} = 0.5$  we find that at  $z = 11$ ,  $R^{2b-sn} \sim 0.6$ , which comes very close to

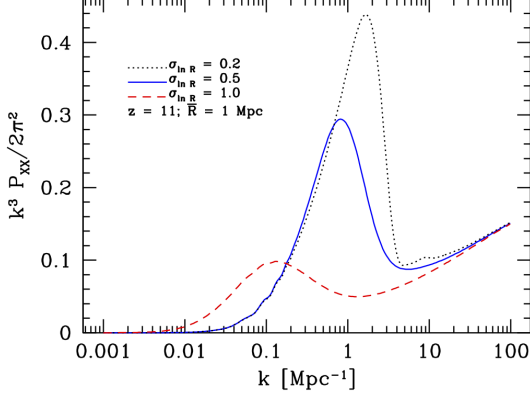


FIG. 16:  $k^3 P_{XX}(k)/2\pi^2$  for  $\bar{R} = 1$  Mpc,  $b = 6$  at different values of  $\sigma_{\ln R}$ .

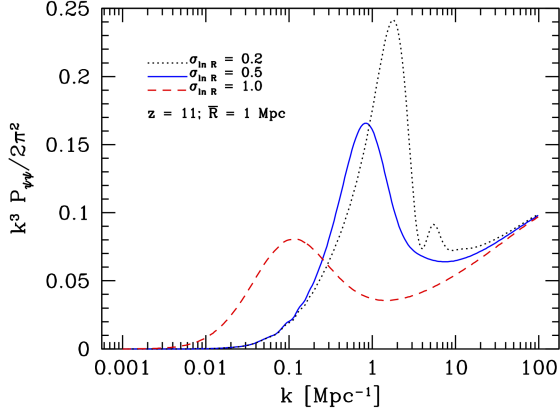


FIG. 17:  $k^3 P_{\psi\psi}(k)/2\pi^2$  for  $\bar{R} = 1$  Mpc,  $b = 6$  at different values of  $\sigma_{\ln R}$ .

what we actually observe in Fig. 7. Note that the ratio depends on the redshift considered, but in general, we find that the 2-bubble term remains of the same order as the shot noise term.

Can the 2-bubble term ever dominate over the 1-bubble term? Since the ratio goes as  $1/\bar{R}^3$  and decreases exponentially in  $\sigma_{\ln R}$ , for bubble distributions with small bubble radius and narrow width, we find that the 2-bubble term can easily dominate the total correlation function. In a more realistic scenario in which the radius and the variance depend on redshift, we expect the 2-bubble term to be increasingly important to the correlation function in the early stages of reionization, in other words, when the correlation function is dominated by points that live in two different bubbles. At the onset of reionization, the bubbles are small and it is more probable to find two points that live in two separate bubbles. As bubbles merge and grow, it becomes more likely that the correlation function has contribution from points that are in the same bubble. The authors in Ref. [6] make this distinction, and divide the reionization model in two

regimes separated by the average ionization fraction.

Concluding, we see that the location of the peak of the correlation function is roughly set by  $k_{peak}$ , given in Eq. (A13), and we note that the location of the peak is almost equivalent for the 1- and 2-bubble terms.

We have shown that in the case of a log-normal distribution the contribution from  $\tilde{P}_{\delta\delta}$  to the peak amplitude is small compared to the shot noise and as such, to the overall correlation. Since the shot noise grows as  $\propto \bar{R}^3$  and exponentially in the width of the distribution  $\sigma_{\ln R}$ , we find that assuming smaller values for these parameters lead to rapidly increasing contribution of the 2-bubble term compared to the 1-bubble term. Since decreasing both of these parameters also increases the value of  $k_{peak}$ , assuming a narrower distribution of bubbles with a smaller average radius results in a correlation function that is dominated by the 2-bubble term and peaks at smaller (physical) scales. These findings are consistent with the expectation that larger bubble imply a larger shot noise.

## 2. Normal distribution

Simulations show that bubbles are well traced by a log-normal distribution at early times [32], while at later times the distribution can transition to a normal distribution. Since at late times, large radii dominate reionization, we expect the shot noise to become more dominant.

A normal distribution is given by

$$P(R) = \frac{1}{\sqrt{2\pi\sigma_R^2}} e^{-(R-\bar{R})^2/(2\sigma_R^2)} \quad (\text{A20})$$

As expected, for a Gaussian, all relevant quantities are much closer to the distribution values (e.g.  $\bar{R}$ ) deviating, by definition, at most 1 sigma.

The average bubble volume is given by

$$\langle V_b \rangle = \frac{4}{3}\pi\bar{R}(\bar{R}^2 + 3\sigma_R^2) \quad (\text{A21})$$

We will assume that a normal distribution is only valid for  $\bar{R} > 1$  Mpc. In this limit, the above equality holds, even for a bound probability function, as long as  $\sigma_R \leq 1$ . This cutoff is consistent with observations. The expression above can easily be understood by Wick expanding the 3-point function  $\langle R^3 \rangle$ .

Similarly, for the variance we obtain:

$$\langle V_b^2 \rangle = \frac{16}{9}\pi^2 (15\bar{R}^4\sigma_R^2 + 45\bar{R}^2\sigma_R^4 + \bar{R}^6 + 15\sigma_R^6) \quad (\text{A22})$$

A gaussian distribution allows us to analytically compute the volume average window function:

$$\langle W_R \rangle(k) = \frac{3e^{-\frac{1}{2}k^2\sigma_R^2} [(k^2\sigma_R^2 + 1) \sin(k\bar{R}) - k\bar{R} \cos(k\bar{R})]}{k^3 (3\bar{R}\sigma_R^2 + \bar{R}^3)}, \quad (\text{A23})$$

At large scales,

$$\lim_{k\bar{R} \ll 1} \langle W_R \rangle = 1, \quad (\text{A24})$$

while at small scales,

$$\lim_{k\bar{R} \gg 1} \langle W_R \rangle = \frac{3\sigma_R^2 e^{-\frac{1}{2}k^2\sigma_R^2} \sin(k\bar{R})}{k\bar{R}(3\sigma_R^2 + 1)} \quad (\text{A25})$$

---


$$\langle W_R^2 \rangle(k) = \frac{9e^{-2k^2\sigma_R^2} \left\{ e^{2k^2\sigma_R^2} [k^2(\bar{R}^2 + \sigma_R^2) + 1] - 2k\bar{R}(2k^2\sigma_R^2 + 1) \sin(2k\bar{R}) + [k^2(\bar{R}^2 - 3\sigma_R^2) - 4k^4\sigma_R^4 - 1] \cos(2k\bar{R}) \right\}}{2k^6(3\bar{R}\sigma_R^2 + \bar{R}^3)^2} \quad (\text{A26})$$


---

At large scales, the variance becomes:

$$\lim_{k\bar{R} \ll 1} \langle W_R^2 \rangle = \langle V_b^2 \rangle / \langle V_b \rangle^2, \quad (\text{A27})$$

and at small scales:

$$\lim_{k\bar{R} \gg 1} \langle W_R^2 \rangle = 9(\bar{R}^2 + \sigma_R^2) / (2k^4(\bar{R}^2 + 3\sigma_R^2)^2) \quad (\text{A28})$$

By equating the two limiting cases, we can derive the peak scale for the variance of  $W_R$ :

$$k_{peak}^{var} = \left[ \frac{9(\bar{R}^2 + \sigma_R^2)(3\bar{R}\sigma_R^2 + \bar{R}^3)}{2(15\bar{R}^4\sigma_R^2 + 45\bar{R}^2\sigma_R^4 + \bar{R}^6 + 15\sigma_R^6)} \right]^{1/4} \quad (\text{A29})$$

The maximum peak value of the shot noise is then given by

$$k^3 P_{X\psi}^{sn} \lesssim (k_{peak}^{var})^3 \frac{\langle V_b^2 \rangle}{\langle V_b \rangle} \quad (\text{A30})$$

A similar approach for the peak scale of the window

The variance is given by:

average does not give an accurate enough answer. Therefore, we will use the following best fit:

$$k_{peak}^{av} \sim 2.2\bar{R}^{-1} \quad (\text{A31})$$

This and the derived maximum value of the shot noise immediately allow us to put a constraint on the ratio between the 2-bubble term and the shot noise,

$$R^{2b-sn} \equiv P_{X\psi}^{2b} / P_{X\psi}^{sn} \simeq b \frac{1 + \bar{x}_H}{1 - \bar{x}_H} \frac{P_{\delta\delta}(k_{peak}^{av})}{\langle V_b \rangle \langle W_R^2 \rangle(k_{peak}^{var})} \quad (\text{A32})$$

From this expression, we find that the shot noise is significantly larger than the 2-bubble term around the peak scale. This nicely fits into the previous picture, since the normal distribution of the bubbles is only physical at late time in the reionization history when  $\bar{R} > 1$  Mpc. At those times the 1-bubble term (dominated by the shot noise) should make up the largest contribution to the total cross-correlation spectrum.

- 
- [1] A. Loeb and R. Barkana, *Ann.Rev.Astron.Astrophys.* **39**, 19 (2001), astro-ph/0010467.
  - [2] X.-H. Fan, M. A. Strauss, R. H. Becker, R. L. White, J. E. Gunn, et al., *Astron.J.* **132**, 117 (2006), astro-ph/0512082.
  - [3] X.-H. Fan, C. Carilli, and B. G. Keating, *Ann.Rev.Astron.Astrophys.* **44**, 415 (2006), astro-ph/0602375.
  - [4] G. Hinshaw, D. Larson, E. Komatsu, D. Spergel, C. Bennett, et al. (2012), 1212.5226.
  - [5] D. Scott and M. J. Rees, *mnras* **247**, 510 (1990).
  - [6] M. McQuinn, O. Zahn, M. Zaldarriaga, L. Hernquist, and S. R. Furlanetto, *Astrophys.J.* **653**, 815 (2006), astro-ph/0512263.
  - [7] P. Madau, A. Meiksin, and M. J. Rees, *Astrophys. J.* **475**, 429 (1997), arXiv:astro-ph/9608010.
  - [8] M. Zaldarriaga, S. R. Furlanetto, and L. Hernquist, *Astrophys.J.* **608**, 622 (2004), astro-ph/0311514.
  - [9] S. Furlanetto, M. Zaldarriaga, and L. Hernquist, *Astrophys.J.* **613**, 16 (2004), astro-ph/0404112.
  - [10] S. Furlanetto, M. Zaldarriaga, and L. Hernquist, *Astrophys.J.* **613**, 1 (2004), astro-ph/0403697.
  - [11] S. Furlanetto, S. P. Oh, and F. Briggs, *Phys.Rept.* **433**, 181 (2006), astro-ph/0608032.
  - [12] A. Lidz, O. Zahn, S. Furlanetto, M. McQuinn, L. Hernquist, et al., *Astrophys.J.* **690**, 252 (2009), 0806.1055.

- [13] R. Wiersma, B. Ciardi, R. Thomas, G. Harker, S. Zaroubi, et al. (2012), 1209.5727.
- [14] M. A. Alvarez, E. Komatsu, O. Dore, and P. R. Shapiro, *Astrophys.J.* **647**, 840 (2006), astro-ph/0512010.
- [15] P. Adshead and S. Furlanetto, *Mon.Not.Roy.Astron.Soc.* (2007), 0706.3220.
- [16] H. Tashiro, N. Aghanim, M. Langer, M. Douspis, S. Zaroubi, et al., *Mon.Not.Roy.Astron.Soc.* **402**, 2617 (2010), 0908.1632.
- [17] H. Tashiro, N. Aghanim, M. Langer, M. Douspis, S. Zaroubi, et al. (2010), 1008.4928.
- [18] G. Holder, I. T. Iliev, and G. Mellema, *Astrophys.J.Lett.* (2006), astro-ph/0609689.
- [19] A. Natarajan, N. Battaglia, H. Trac, U. L. Pen, and A. Loeb (2012), 1211.2822.
- [20] C. Dvorkin, W. Hu, and K. M. Smith, *Phys.Rev.* **D79**, 107302 (2009), 0902.4413.
- [21] C. Dvorkin and K. M. Smith, *Phys.Rev.* **D79**, 043003 (2009), 0812.1566.
- [22] V. Gluscevic, M. Kamionkowski, and D. Hanson (2012), 1210.5507.
- [23] K. Masui, E. Switzer, N. Banavar, K. Bandura, C. Blake, et al. (2012), 1208.0331.
- [24] E. Chapman, F. B. Abdalla, J. Bobin, J.-L. Starck, G. Harker, et al. (2012), 1209.4769.
- [25] G. Harker, S. Zaroubi, G. Bernardi, M. A. Brentjens, A. de Bruyn, et al., *Mon.Not.Roy.Astron.Soc.* **405**, 2492 (2010), 1003.0965.
- [26] G. Mellema, L. Koopmans, F. Abdalla, G. Bernardi, B. Ciardi, et al. (2012), 1210.0197.
- [27] A. Liu, M. Tegmark, J. Bowman, J. Hewitt, and M. Zaldarriaga (2009), 0903.4890.
- [28] A. Liu, J. R. Pritchard, M. Tegmark, and A. Loeb (2012), 1211.3743.
- [29] X. Wang and W. Hu, *Astrophys.J.* **643**, 585 (2006), astro-ph/0511141.
- [30] G. B. Field, *Proceedings of the Institute of Radio Engineers.* **46**, 240 (1958).
- [31] A. Lewis, A. Challinor, and A. Lasenby, *Astrophys.J.* **538**, 473 (2000), astro-ph/9911177.
- [32] O. Zahn, A. Lidz, M. McQuinn, S. Dutta, L. Hernquist, et al., *Astrophys.J.* **654**, 12 (2006), astro-ph/0604177.
- [33] A. Liu and M. Tegmark, *Mon.Not.Roy.Astron.Soc.* **419**, 3491 (2012), 1106.0007.
- [34] A. Kogut, J. Dunkley, C. Bennett, O. Dore, B. Gold, et al., *Astrophys.J.* **665**, 355 (2007), 0704.3991.
- [35] L. La Porta, C. Burigana, W. Reich, and P. Reich (2008), 0801.0547.
- [36] P. Shaver, R. Windhorst, P. Madau, and A. de Bruyn (1999), astro-ph/9901320.
- [37] M. G. Santos, A. Cooray, and L. Knox, *Astrophys.J.* **625**, 575 (2005), astro-ph/0408515.
- [38] X.-M. Wang, M. Tegmark, M. Santos, and L. Knox, *Astrophys.J.* **650**, 529 (2006), astro-ph/0501081.
- [39] M. F. Morales, *Astrophys.J.* **619**, 678 (2005), astro-ph/0406662.
- [40] Y. Mao, M. Tegmark, M. McQuinn, M. Zaldarriaga, and O. Zahn, *Phys.Rev.* **D78**, 023529 (2008), 0802.1710.
- [41] 713764 (2006), astro-ph/0604069.
- [42] M. Niemack, P. Ade, J. Aguirre, F. Barrientos, J. Beall, et al., *Proc.SPIE Int.Soc.Opt.Eng.* **7741**, 77411S (2010), 1006.5049.
- [43] J. Austermann, K. Aird, J. Beall, D. Becker, A. Bender, et al., *Proc.SPIE Int.Soc.Opt.Eng.* **8452**, 84520E (2012), 1210.4970.
- [44] M. Zaldarriaga, L. Colombo, E. Komatsu, A. Lidz, M. Mortonson, et al. (2008), 0811.3918.
- [45] M. Su, A. P. Yadav, M. McQuinn, J. Yoo, and M. Zaldarriaga (2011), 1106.4313.
- [46] H. V. Peiris and D. N. Spergel, *Astrophys.J.* **540**, 605 (2000), astro-ph/0001393.
- [47] M. Tegmark, A. Taylor, and A. Heavens, *Astrophys.J.* **480**, 22 (1997), astro-ph/9603021.
- [48] M. J. Mortonson and W. Hu, *Astrophys.J.* **657**, 1 (2007), astro-ph/0607652.
- [49] O. Zahn, A. Mesinger, M. McQuinn, H. Trac, R. Cen, et al. (2010), 1003.3455.